

Understanding glass-like Vogel-Fulcher equilibration times: microcanonical effective temperatures in quenched 3D martensites

N. Shankaraiah¹, K.P.N. Murthy² and S.R. Shenoy¹

¹Tata Institute of Fundamental Research-Hyderabad, Hyderabad, Telangana 500046, India.

²Dept of Physics, Central University of Rajasthan, Bandar Sindri, Rajasthan 305817, India

(Dated: December 7, 2021)

We do Monte Carlo simulations of four 3D structural transitions through vector-spin models of martensitic strain domains, to test a generic post-quench Partial Equilibration Scenario (PES) of Ritort. We indeed find that the PES distribution from locating downward passages between fixed-energy shells, has an exponential tail in heat releases scaled in an effective search temperature. A linear vanishing of this $T_{eff}(T) \sim T_d - T$ at a temperature T_d where passage-searches freeze, explains the Vogel-Fulcher divergence of equilibration times extracted from martensitic alloy data.

How do systems re-equilibrate after a quench? For thermal quenches to a low temperature T , activated jumps over energy barriers ΔU are relatively rarer. Sets of competing rates are dominated by *entropy* barriers $S_B > 0$ to finding re-equilibration pathways at almost constant energy, $\{e^{-(\Delta U - T\Delta S)/T}\} \rightarrow \{e^{\Delta S} \equiv e^{-S_B}\}$.

Ritort and coworkers¹⁻⁴ have proposed a Partial Equilibration Scenario (PES) for re-equilibrations dominated by entropy barriers. Over a waiting time t_w , a post-quench aging system rapidly explores configurations of energy $E(t_w)$, entropy $S(E)$, and (inverse) microcanonical effective temperature $1/T_{eff}(t_w) \equiv dS(E)/dE$. Passages to a lower shell of $E(t_w + 1) \equiv E' = E(t_w) + \delta E$ are driven by intermittent spontaneous energy releases ($\delta E < 0$) to the heat bath at T . The PES says that an iteration of these aging steps ratchets the system down to the new canonical equilibrium. The non-equilibrium probability distribution for energy changes^{1,4} $P_0(\delta E; t_w)$ is peaked at positive energies, with an exponential tail for $\delta E < 0$ whose fall-off $\sim e^{\delta E/2T_{eff}(t_w)}$ determines the effective temperature. The PES heat-release $dQ = \delta E$ distribution has been studied, by analytic Monte Carlo (MC) methods for harmonic oscillators³, and by numerical MC simulations of spin glasses and Lennard-Jones liquids^{2,4}.

Equilibration times of supercooled liquids and colloidal crystals⁵⁻⁸ rise steeply above a glass temperature T_G , as a Vogel-Fulcher-Tamann (VFT) form⁷ $\sim e^{1/T - T_G}$, with unusual time decays and frequency responses⁸. Although structural glass freezing^{5,6} that pre-empts crystallization⁹ has been investigated for more than a century, it is still not fully understood. The study of quenches below the solid-solid structural transitions of martensites¹⁰⁻¹⁷, that also have unusual time evolutions^{11,12}, may contribute to an understanding.

Martensites undergo first-order, diffusionless⁹ transitions¹⁰ from the higher-symmetry austenite, with atomic shifts fixed by their unit-cell distortions ('military transformations'). The order-parameter strains have degenerate lower-symmetry 'variants' separated by crystallographically oriented Domain Walls (DW), that can form complex textures in strain, and in strain-coupled functional variables¹⁷. A long-standing puzzle^{11,12} is that while austenite quenched to below

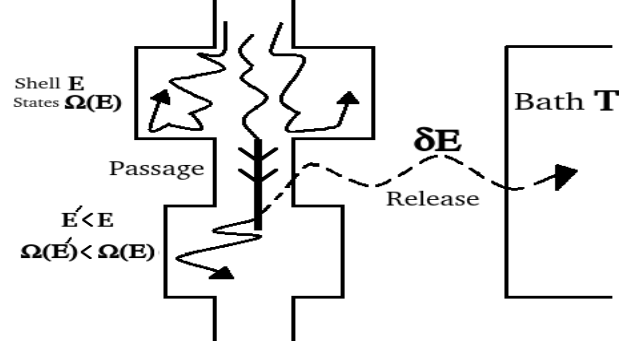


FIG. 1. Schematic of Partial Equilibration Scenario, plus postulated passage-constraints: The system in a configurational shell of states $\Omega(E)$ with energy E , makes a passage to the next shell of fewer states $\Omega(E')$ with $E' < E$. There are slow stochastic heat releases $\delta E \equiv E' - E < 0$ to the bath at T , on crossing the entropy barriers $S_B \equiv -\Delta S = -\ln[\Omega(E')/\Omega(E)] > 0$. In our specific case of quenches below a first-order transition, the passages can be *constrained*, by required order parameter events. The turned-back wiggly lines are failed passage attempts. The straight bold-line denotes successful attempts. We postulate T -dependent passage constraints, eg the order parameter Fourier profile must distort to enter a k -space Golf Hole (GH), that funnels into fast passage. A pinch-off of GH entry at a $T = T_d$ induces VFT divergences of passage delay times $\sim e^{1/T - T_d}$.

an (athermal) martensite start temperature M_s results in sudden martensitic conversions, quenches to *above* M_s , show slow conversions instead of no conversions. When T increases by a few percent closer to a delay divergence temperature T_d , the delays rise sharply from a few, to ten thousand seconds¹². To be more relevant for actual experiments, we consider simulations in *three* dimensions with vector order parameters, such as in the cubic-tetragonal (CT) transition¹⁵. There is a two-component strain order parameter $N_{OP} = 2$, with three competing unit-cell 'variants' $N_V = 3$. (Using this notation, the Ising model has $N_{OP} = 1, N_V = 2$.)

In this Letter we study the equilibration of 3D athermal martensites for four structural transitions in MC simulations, confirming the generic PES, and its effective

temperature that regulates heat releases¹⁻⁴. We apply PES ideas to quenches across a first order transition. The Order Parameter (OP) rises from zero, enabling the waiting time t_w to be defined by rising-OP marker events, dependent on T . This choice¹⁶ $t_w = t_m(T)$ induces quench temperature dependences in PES distributions: $T_{eff}(t_w) \rightarrow T_{eff}(T)$ and $P_0(\delta E; t_w) \rightarrow P_0(\delta E, T)$. For passages to lower energy shells, as in Fig 1, the OP evolution must satisfy T -controlled, delay-inducing passage constraints, postulated as of two possible types: a) A constraint that OP configurations must find and enter a Golf Hole (GH) that funnels into fast passage, as suggested for protein folding¹⁸; or b) A constraint that the OP states must encounter transient catalysts that enable fast passages, as inspired by facilitation models¹⁹⁻²¹. Our case is a), and we find a linear vanishing $T_{eff}(T) \sim (T_d - T)$. The ‘search freezing’ temperature T_d occurs at a pinch-off of the \vec{k} -space *inner* radius of a modulated GH. Equilibration times are exponential in entropy barriers, and hence show divergences of the VFT form $\bar{t}_m(T) \sim e^{1/T_{eff}(T)} \sim e^{1/|T-T_d|}$. Conversely, entropy barriers vanish and delay times collapse, when the GH is comparable to the Brillouin zone. The predicted divergence/collapse of conversion times is confirmed by data extracted from simulations²² and from experiment^{11,12}.

The four chosen structural transitions^{15,22} occur in materials with useful functionalities¹⁷. The transitions are: tetragonal-orthorhombic (YBCO, superconductivity); cubic-tetragonal (FePd, shape memory); cubic-orthorhombic (BaTiO, ferroelectrics); cubic-trigonal (LaSrMnO, colossal magnetoresistance).

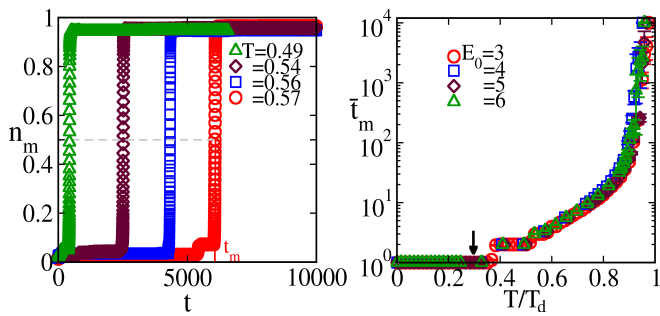


FIG. 2. Delay times for CT martensitic conversion: The martensite fraction $n_m(t_m) = 0.5$ defines t_m . a) For $T \leq T_1$ conversions are immediate, at $t_m = 1$. For $T_d > T > T_1$ DW sluggishness causes an incubation delay $t_m(T)$ that postpones the conversion avalanche. b) Log-linear plot of mean delay time $\bar{t}_m(T)$ versus $T/T_d < 1$. Delay times are not activated, since not exponentially sensitive to Hamiltonian energy scales E_0 : delays are from *entropy* barriers. [The vertical axis is of Natural logs, but numerical tics are powers of 10.]

To plausibly link simulations to experiment, we must show the model Hamiltonians comes from material symmetries. The discretized-strain Hamiltonian¹⁵ in 3D is obtained from a crystal-symmetry invariant strain free energy F , that has physically required Compatibility¹⁴,

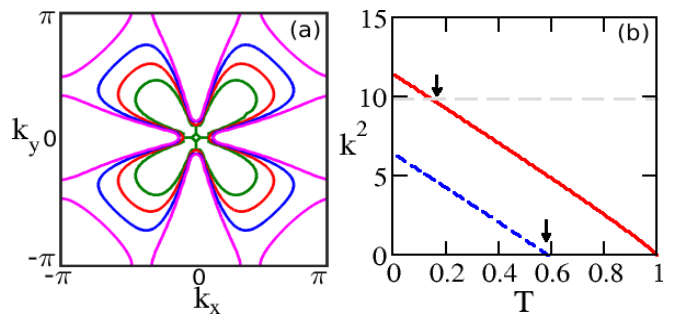


FIG. 3. *Golf Holes for CT transition*: The temperature dependence of GH size and shape is shown for a $[1,1,1]$ slice of anisotropic Golf Holes in 3D Fourier space. a) The GH shapes in (k_x, k_y) vary with T , and shrink on warming. The open butterfly GH changes topology to a segmented four-petal flower around T_d . b) The GH inner and outer radii k_{in}, k_{out} are plotted as bending energies \bar{k}^2 vs T . The outer radius $k_{out}(T)$ exceeds a Brillouin Zone size of $\sim \pi$ (horizontal dashes), for $T \leq T_1$ (arrow) so conversions are immediate; and becomes a $k^2 = 0$ point at the thermodynamic transition to austenite at $T_0 = 1$. The inner radius $k_{in}(T)$ vanishes earlier, at $T_d < T_0$ (arrow) where conversion times diverge.

Ginzburg and Landau terms in $F/E_0 = \sum_{\vec{r}, \vec{r}'} f_C + \sum_{\vec{r}} [f_G + f_L]$. There are six independent *physical* strains¹⁵ in 3D, that are linear combinations of Cartesian-component strains: compressional e_1 ; deviatoric or rectangular e_2, e_3 , and shear e_4, e_5, e_6 . The OP of the $N_{OP} = 2$ cubic-tetragonal (CT) transition are two deviatoric strains $\vec{e} = (e_3, e_2) = (\frac{1}{\sqrt{6}}\{e_{xx} + e_{yy} - 2e_{zz}\}, \frac{1}{\sqrt{2}}\{e_{xx} - e_{yy}\})$, of the variants. The austenite phase is $\vec{e} = \vec{0}$.

The remaining $6 - N_{OP}$ non-OP strains (one compressional and three shears) enter the Hamiltonian as harmonic energies. These are minimized subject to a linear St Venant Compatibility constraint¹⁴ that says no dislocations are generated: the double-curl of the strain tensor must vanish. There are three independent algebraic equations in \vec{k} space, connecting OP and non-OP strains¹⁵. The non-OP harmonic energies then analytically yield an OP-OP interaction, whose transition-specific, *anisotropic*⁶ Compatibility kernel¹⁵ is a 2X2 matrix, $U_{\ell\ell'}(\hat{k})$ where $\ell, \ell' = 2, 3$. There is a prefactor of $(1 - \delta_{\vec{k}, 0})$, and dependence on direction $\hat{k} = \vec{k}/|\vec{k}|$.

The Landau free energy for CT is $f_L(\vec{e}) = [(\tau - 1)\vec{e}^2 - 2(e_3^3 - 3e_3e_2^2) + \vec{e}^4]$ and has 4 minima, at $N_V = 3$ variants plus at zero strain. Here $\tau(T) \equiv (T - T_c)/(T_0 - T_c)$, and $\tau(T_c) = 0$ at the spinodal T_c , while $\tau(T_0) = 1$ at the first-order transition temperature, that is scaled to be unity $T_0 = 1$. The characteristic temperatures in decreasing order are $T_0 = 1 > T_d > T_c > M_s$.

In polar coordinates $\vec{e} \equiv |\vec{e}|\vec{S}$. Here the unit-magnitude ‘variant vectors’ $\vec{S}(\vec{r})$ specify the unit-cell variants on either side of a Domain Wall (DW) (that can be martensite-martensite or martensite-austenite). The nonzero $N_V = 3$ martensite-variants have spins¹⁵ $\vec{S} =$

$(S_3, S_2) = (1, 0), (-1/2, \sqrt{3}/2), (-1/2, -\sqrt{3}/2)$, pointing to corners of an equilateral triangle in a unit circle, while the centroid $\vec{S} = (0, 0)$ is austenite.

The degenerate Landau minima are at mean-OP magnitudes $\bar{\varepsilon}(T) = (3/4)[1 + \sqrt{1 - (8\tau/9)}]$. The variant domains have mostly-flat strain magnitudes, approximated by $\bar{\varepsilon}(T)$. Substituting $\vec{\varepsilon}(\vec{r}) \rightarrow \bar{\varepsilon}(T)\vec{S}(\vec{r})$, the Landau term becomes $f_L(\vec{\varepsilon}) \rightarrow f_L(T)\vec{S}(\vec{r})^2$. Here $f_L(T) \equiv \bar{\varepsilon}(T)^2 g_L(T) \leq 0$, where $g_L = (\tau - 1) + (\bar{\varepsilon}(T) - 1)^2 \leq 0$. At $T = T_0^-$, the OP is unity $\bar{\varepsilon} = 1$ and $g_L = 0$.

Notice a natural separation of response time scales to T quenches: the OP magnitude $\bar{\varepsilon}(T)$ responds immediately, while Domain Walls evolve in hundreds or thousands of time steps t , successively from DW Vapour to DW Liquid to a DW Crystal of twins. See Videos²⁰ A,B. For shallow quenches $T_0 > T > T_1$, the DW Vapour-to-Liquid conversion has the long delays studied here. [For deeper quenches $T \ll T_1$, it is the DW Liquid-to-Crystal evolution that has long orientation delays to regular twins. See Video²⁰ C.] The DW moves by correlated flips of spins that bracket it, while domain spins remain locked, so there is dynamical heterogeneity in space and time.

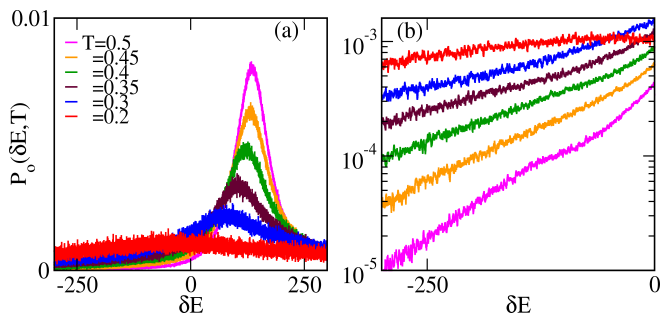


FIG. 4. Energy-change statistics for CT transition: a) Linear-linear plot of the normalized probability $P_0(\delta E, T)$ versus energy change δE , for six T quenches. b) Log-linear version. Slope at the origin $\beta_{eff}(T)/2$ rises from zero for $T > T_1$.

The total hamiltonian is $\beta H = \beta H_C + \beta H_G + \beta H_L$, without extrinsic disorder. It is diagonal in Fourier space,

$$\beta H = \frac{D_0}{2} [\sum_{\ell, \ell'} \sum_{\vec{k}} \{\epsilon_{\ell, \ell'}(\vec{k}) \vec{S}_{\ell}(\vec{k}) \vec{S}_{\ell'}^*(\vec{k})\}], \quad (1)$$

with $D_0 \equiv 2\bar{\varepsilon}(T)^2 E_0/T$. The spectrum, with $K_{\mu}(\vec{k}) \equiv 2 \sin(k_{\mu}/2)$ and $\mu = x, y, z$, is

$$\epsilon_{\ell, \ell'}(\vec{k}) \equiv \{g_L(T) + \xi_0^2 \vec{k}^2\} \delta_{\ell, \ell'} + \frac{A_1}{2} U_{\ell \ell'}(\hat{k}). \quad (2)$$

The Landau term $H_L \sim g_L < 0$ and the Ginzburg term $H_G \sim \vec{k}^2 > 0$ have competing signs. The Compatibility term $\beta H_C > 0$ has an anisotropic kernel that orients the Domain Walls^{14-16,23}. The $\ell = \ell'$ kernel $U_{\ell, \ell}(\hat{k})$ has a minimum value $U_{\ell, \ell}(min) = 0$ for the most favoured orientation, and a maximum value $U_{\ell, \ell}(max)$ for most disfavoured. The kernels for the four 3D transitions are in the Appendix of Ref 15.

In MC simulations, the initial state $t = 0$ is high-temperature austenite that is randomly and dilutely (2%) seeded with martensite unit-cells. Typical parameters are $T_0 = 1$; $\xi_0^2 = 1$; $T_c = 0.81$; $E_0 = 3$; system volume $L^3 = 16^3$; $N_{runs} = 100$; and holding times $t_h = 10^4$ MC sweeps. The martensite fraction is $n_m(t) \equiv \frac{1}{N} \sum_{\vec{r}} S^2(\vec{r}, t) \leq 1$, with $n_m = 0$ or 1 for uniform austenite or martensite. The conversion time t_m is defined as when¹⁶ $n_m(t_m) = 1/2$. An athermal martensite droplet or embryo can form anywhere, and after waiting for $t_w = t_m$, can propagate rapidly to the rest of the system¹³. Hence it is mean rates \bar{r}_m (or inverse times), that are averaged over runs, analogous to total resistors in parallel determined by the smallest resistance. Mean times \bar{t}_m are inverse mean rates: $\bar{t}_m(T) \equiv 1/\bar{r}_m(T)$.

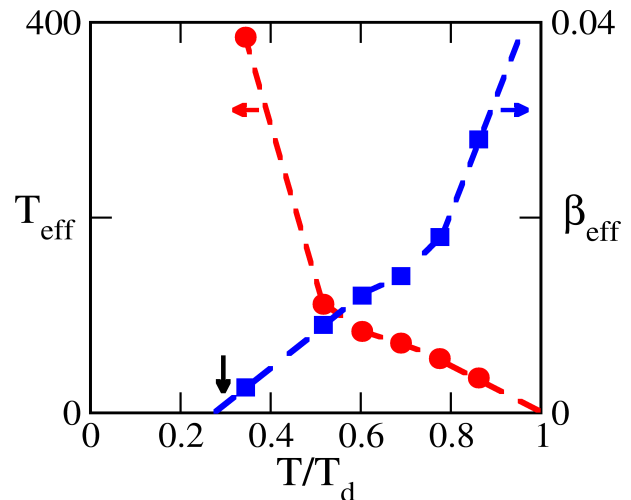


FIG. 5. Effective temperature and its inverse, versus quench temperatures for CT transition: Left vertical axis: $T_{eff}(T)$ versus T/T_d appears to vanish as $\sim (T_d - T)$, and rises from $T_1 < T_d$. Right vertical axis: $\beta_{eff}(T)$ appears to vanish as $\sim (T - T_1)$, and rises rapidly near $T_d > T_1$. The entropy barrier $S_B \sim \beta_{eff}$ will then vanish or diverge at T_1 (downward arrow) or at T_d . Dashed lines are guides to the eye.

The MC procedure is standard, but with a crucial extra data retention^{1,2,4} of energy changes.

0. Take $N = L^3$ sites, each with a vector spin of N_{OP} components, in one of $N_V + 1$ possible values (including zero) at MC time t . Each $\{\vec{S}(\vec{r})\}$ set is a ‘configuration’.
1. Randomly pick one of N sites, and randomly flip the spin on it to a new direction/value, and find the (positive/negative) δE to reach the new configuration.
2. If the energy change $\delta E \leq 0$, then accept the flip. If $\delta E > 0$, then accept flip with probability $e^{-\delta E/T}$. Record this δE , that is not usually retained after use.
3. Repeat steps 1 and 2. Stop after N such spin-flips. This configuration has the conversion fraction $n_m(t + 1)$.
4. We collect²² all $\{\delta E\}$ from each spin-flip (configuration change) within each MC sweep of every run, for all times up to $t_w \leq t_m(T) \leq t_h$. The set size $N \times t_m \times N_{run}$ has up to $16^3 \times 10^4 \times 100$ data points. We take six

quenches, from $T = T_1$ upwards towards T_d .

Figure 2a shows $n_m(t)$, the martensite conversion-fraction in a *single* run, versus MC time t for different temperatures T . For quenches $T \leq T_1$, avalanche conversions, characteristic of athermal martensite, occur in the very first sweep over all spins ($t = 1$). We identify T_1 with the martensite start temperature^{11,12}, $M_s = T_1$. For higher temperatures $T > T_1$, there is a curious ‘incubation’ period when seemingly nothing happens^{16,20} until a waiting time $t_w = t_m$, brings on a postponed avalanche. Fig 2b shows that the mean incubation delays rise steeply, as T approaches a temperature T_d .

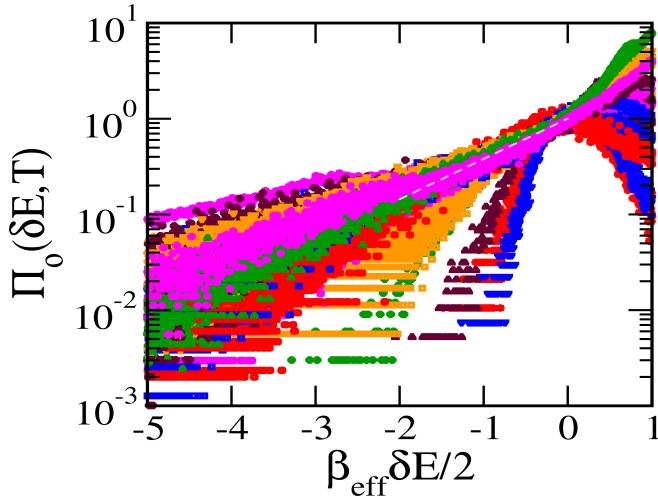


FIG. 6. *Universal slope of PES distribution:* Log-linear scaled plot of $\Pi_0(\delta E, T) \equiv P_0(\delta E, T)/P_0(0, T)$ versus $z \equiv \beta_{eff}(T)\delta E/2$. The PES predicts a universal slope of unity at $z = 0$. The four transitions mentioned have respective slope averages and standard deviations of 1.000 ± 0.045 , 1.025 ± 0.036 , 1.009 ± 0.08 , 0.850 ± 0.085 . The data for six T and four transitions have mean slope (dashed white line) of 0.97 ± 0.06 .

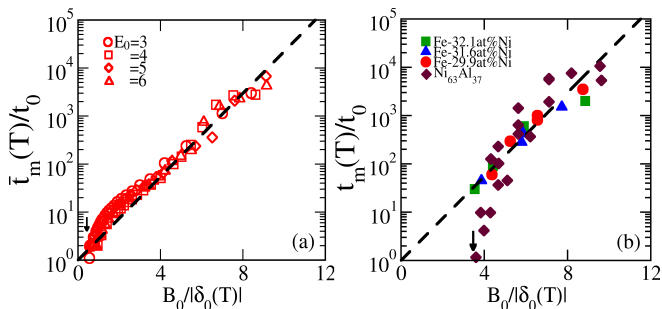


FIG. 7. *Log-linear plots of scaled time versus (inverse) scaled temperature deviation:* Scaled conversion times t_m/t_0 versus $B_0/|\delta_0|$ with parameters t_0, B_0 extracted from data. There is Vogel Fulcher linearity near T_d , with falloffs near T_1 (downward arrows). a) From CT simulations in 3D for different E_0 . b) From experiments^{11,12} in 3D for different alloys.

We use protein-folding concepts such as Golf Holes and

Funnels¹⁸, to understand the conversion delays. Suppose a protein model in terms of ball-spring-hinge variables is diagonalized in eigen-modes with eigen-labels $\vec{\alpha}$ and energy spectrum $\epsilon(\vec{\alpha})$. Then $\epsilon(\vec{\alpha}) = 0$ in $\vec{\alpha}$ -space defines a zero-energy Golf Hole (GH) contour, with a negative-energy Funnel region inside it. An isotropic spectrum $\epsilon(|\vec{\alpha}|) = 0$ yields a spherical-surface GH, as in a protein folding model¹⁸ with a three-component $\vec{\alpha}$.

For our model, setting the spectrum equal to zero $\epsilon_{\ell,\ell}(\vec{k}) = 0$ defines an *anisotropic* surface in \vec{k} -space that is the boundary of the 3D GH. For the CT case, a $[1,1,1]$ slice intersects the GH surface as an open, butterfly-shaped locus with an inner and outer radius, inside the Brillouin Zone (BZ). See Fig 3. The outer radius has $k_{out}(T)^2 = |g_L(T)|$, that vanishes at $T = T_0$, when the GH is a point. For $T \leq T_1$, the radius $k_{out}(T)$ is larger than a BZ scale $\sim \pi$, and martensitic passages are immediate. The inner radius has $k_{in}(T)^2 = |g_L(T)| - (A_1/2)U_{\ell,\ell}(max)$, that pinches off at a $T_d < T_0$ where the GH changes to a *segmented* four-petaled flower. Passages are energetically open, but topologically blocked. Lower-energy PES shells are available, but not accessible.

We collect the $O(1)$ changes $\{\delta E\}$ to the $O(N)$ energy E . The probability $P_0(\delta E, T)$ to access E' from E , is proportional to the number of target states $\Omega(E')$. With $S(E') = \ln \Omega(E')$, the probability ratio $R_0(\delta E)$ of energy changes is related to the entropy change $\Delta S(\delta E) \equiv S(E') - S(E) < 0$ by a fluctuation relation for aging¹⁻⁴:

$$R_0 \equiv P_0(\delta E, T)/P_0(-\delta E, T) = \Omega(E')/\Omega(E) = e^{\Delta S(\delta E)}. \quad (3)$$

Entropy barriers $S_B \equiv -\Delta S$ rise, when the searched-for states become rarer (key seeks lock, most attempts fail). Since $R_0(\delta E)R_0(-\delta E) \equiv 1$, the entropy change is odd, $\Delta S(\delta E) + \Delta S(-\delta E) = 0$, and a solution is

$$P_0(\delta E, T) = P_0^{(+)}(\delta E) e^{\frac{1}{2}\Delta S(\delta E)}, \quad (4)$$

with an even $P_0^{(+)}(\delta E) \equiv \sqrt{P_0(\delta E, T) P_0(-\delta E, T)}$. The leading term in the entropy-change for small heat releases is $\Delta S \simeq \beta_{eff}\delta E$ where $\beta_{eff} \equiv 1/T_{eff}$. For $\delta E = -|\delta E| < 0$, the Boltzmann-like form $P_0 \simeq e^{-\frac{1}{2}\beta_{eff}(T)|\delta E|}$ gives a physical meaning to the effective temperature, as a *search range* of accessible energy shells. If $\beta_{eff} \rightarrow 0$, entropy barriers collapse, and passages are immediate. If $T_{eff} \rightarrow 0$, then entropy barriers diverge, and passages cease. Glassy freezing is a shutdown of PES searches.

Fig 4a shows that, as in PES models¹⁻⁴, the $P_0(\delta E, T)$ peaks are at positive δE , understood as a completion-of-square between a gaussian peaked at the origin and an exponential tail for $\delta E < 0$. Fig 4b shows behaviour near the origin, where the slopes define $\frac{1}{2}\beta_{eff}(T)$.

Fig 5 shows the dependence of $\beta_{eff}(T)$ and $T_{eff}(T)$ on the quench temperature T . The data suggest there is a linear vanishing of $T_{eff} \simeq (1/B_0)|T - T_d|$ near a search freezing at T_d , and also a vanishing of $\beta_{eff} \sim |T - T_1|$ near a search avalanche at T_1 .

Fig 6 shows log-linear plots for a scaled $\Pi_0(\delta E, T) \equiv P_0(\delta E, T)/P_0(0, T)$ versus the entropy-barrier related variable $\frac{1}{2}\beta_{eff}\delta E$. See also Figure insets, Ref 4. Data are for four 3D structural transitions, and six T between the collapse and divergence of entropy barriers.

If the mean conversion time is exponential in the entropy barrier, then near T_d we have $\bar{t}_m(T) \simeq t_0 e^{B_0/|\delta_0(T)|}$, where the constants B_0, t_0 can be fixed by simulational and experimental data²². The initial slope in $|\delta_0|$ of $1/\ln \bar{t}_m(T)$ gives $1/B_0$; and the extrapolated intercept of $\ln \bar{t}_m(T)$ versus $1/|\delta_0(T_0)|$ gives t_0 . For Ni-Al data¹¹ the ‘fragility’ parameter⁵ $B_0 T_d = 1.23$ Kelvin, and the austenite-martensite DW time scale is $t_0 = 1$ sec.

Fig 7a shows that CT times show VFT behaviour near T_d and fall-off behaviour near T_1 . Fig 7b shows data extracted from Ni-Al and Fe-Al alloys^{11,12} are similar.

In summary, post-quench aging in athermal martensites shows characteristic signatures of the Partial Equilibrium Scenario. The VFT behaviour found in 3D sim-

ulations/ experiments is understood as a consequence of a linearly vanishing PES search temperature.

Further model simulations under deeper quenches could study if facilitation constraints of vanishing lifetimes of transient catalysts^{20,21} could induce DW glass freezing. Further experimental work on martensitic alloys^{11,12} could record signal and noise under systematic quench steps of $1/|\delta_0|$, over the delay region $T_d > T > T_1$; as well as the precursor^{14,20} region $T_0 > T > T_d$ above it. The distributions of intermittent energy releases could be measured through their concurrent resistive, photonic, acoustic, and elastic signals^{11,12,24}. Finally, quenches of complex oxides^{17,23} near their structural/functional transitions, might similarly induce¹ PES aging in their (strain-coupled) functional variables.

Acknowledgement: It is a pleasure to thank Smarajit Karmakar for valuable discussions on the glass transition.

-
- ¹ F.Ritort, J.Phys. Chem B **108**, 6893 (2004); and in *Unifying Concepts in Granular Media and Glasses*, (eds.) A. Coniglio, A. Fierro, H.J. Hermann and M. Nicodemi, Elsevier (2004); arXiv/ condmat/ 03113710v1.
- ² A. Crisanti and F. Ritort, Europhys. Lett., **66**,253 (2004).
- ³ L. L. Bonilla, F.G. Padilla and F. Ritort, Physica A **250**, 315 (1998);
L. Garriga and F. Ritort, Phys. Rev. E **72**, 031505 (2005).
- ⁴ A. Crisanti, M. Pecco and F. Ritort, Phys. Rev. Lett., **110**, 080601 (2013).
- ⁵ K. Binder, W. Kob, *Glassy Materials and Disordered Solids*, World Scientific, Singapore (2005);
A.L. Greer, K.F. Kelton, S. Sastry, Eds., *Fragility of glass-forming liquids*, Hindustan Book Agency, New Delhi (2014). A VFT time $\sim e^{1/(T-T_G)}$ written as $e^{E_B(T)/T}$ suggests a diverging activation energy barrier. Written as $e^{-\Delta S(T)} \simeq e^{1/T_{eff}(T)}$, it suggests a diverging entropy barrier through the linear vanishing of an effective temperature, from a closing bottleneck.
- ⁶ P. Harrowell, Nature Phys **2**, 157 (2006); H. Shintani and H. Tanaka, Nature Phys **2**, 200 (2006);
X. Yang, H. Tong, W-H. Wang, and K. Chen, Phys. Rev. E, **99**, 062610 (2019).
- ⁷ P. Lunkenheimer, S. Kastner, M. Koehler and A. Loidl, Phys. Rev. E **81**, 051504 (2010).
- ⁸ R. Boehmer, K.L. Ngai, C.A. Angell, D.J. Plazek, J. Chem. Phys., **99**, 4201 (1993); T.V. Ramakrishnan and M. Raj Lakshmi, Eds., *Non-Debye relaxation in condensed matter*, World Scientific, Singapore (1987).
- ⁹ H. Fang, M.F. Hagan, W.B. Rogers, Proc. Nat. Acad. Sci., **117**, 27927 (2020).
- ¹⁰ K. Bhattacharya, *Microstructure of Martensite*, Oxford University Press (2003).
- ¹¹ T. Kakeshita, T. Fukuda and T. Saburi, Scripta Mat. **34**, 1 (1996); T. Kakeshita, K. Kuroiwa, K. Shimuzu, T. Ikeda, A. Yamagashi, and M. Date, Mat. Trans. JIM, **34**, 423 (1993).
- ¹² M. Aspelmeier, U Klemradt, L.T. Wood and S.C. Moss, Phys. Stat. Sol. (a) **174**, R9 (1999);
L. Müller , U. Klemradt, T.R. Finlayson, Mat. Sci. and Eng. A **438**, 122 (2006);
L. Müller, M. Waldorf, G. Gutt, G. Grubel, A. Madsen, T. R. Finlayson and U. Klemradt, Phys. Rev. Lett., **109**,105701 (2011).
- ¹³ P.R. Rios and J.R.C. Guimaraes, Scripta Mat., **57**, 1105 (2007);
P.R. Rios, F.G. Cardoso, T.A. Neves and J.R.C. Guimaraes, in the Minerals, Metals and Materials Society, TMS 2015 144th Annual Meeting, Cham, Springer (2015), https://doi.org/10.1007/978-3-319-48127-2_84.
- ¹⁴ S. Kartha, J. A. Krumhansl, J. P. Sethna, and L. K. Wickham, Phys. Rev. **B** 52, 803 (1995).
- ¹⁵ S.R. Shenoy, T. Lookman and A. Saxena, Phys. Rev. B **82**, 144103 (2010). See Appendix for the four Compatibility kernels in 3D.
K.O. Rasmussen, T. Lookman, A. Saxena, A.R. Bishop, R.C. Albers and S.R. Shenoy, Phys. Rev. Lett., **87**, 055704 (2001).
- ¹⁶ N. Shankaraiah, K. P. N. Murthy, T. Lookman and S. R. Shenoy, Europhys. Lett. **92**, 36002 (2010);
Phys. Rev. B **84**, 064119 (2011); Phys. Rev. B **91**, 214108 (2015).
- ¹⁷ W.I.F. David, C.C. Wilson, P. P. Edwards, R. Jones, M.R. Harrison, Nature **331**, 245 (1988);
V. Hardy, A. Maignan, S. Hebert, C. Yaicle, C. Martin, M. Hervieu, M.R. Lees, G. Rowlands, D. McK. Paul and B. Raveau, Phys. Rev. B **68**, R220402 (2003);
V. Hardy, S. Majumdar, S.J. Crowe, M.R. Lee, D. McK. Paul, L. Herve', A. Maignan, S. Hebert, C. Martin, C. Yaicle, M. Hervieu and B. Raveau, Phys. Rev. B **9**, 020407 (R) (2004);
V. Podzorov, B.G. Kim, V. Kiryukin, M.E. Gershenson and S.W. Cheong, Phys. Rev. B **64**, 140406 (R) (2001);
V Podzorov, C.H. Chen, M.E. Gershenson and S.-W. Cheong, Europhys. Lett., **55**, 411 (2001).
- ¹⁸ D. J. Bicout and A. Szabo, Protein Science **9**, 452 (2000);
P.G. Wolynes, Proc. of the Am. Phil. Society **145**, 4 (2001);
M. Cieplak and J.I. Sulkowska, J. Chem. Phys., **123**,194908

(2005).

¹⁹ F. Ritort and P. Sollich, Adv. Phys. **52**, 219 (2003).

²⁰ Supplementary Material. [URL]

Videos for the 2D square-rectangle $N_{OP} = 1, N_V = 2$ transition, with austenite (green) and the two martensite variants (red/ blue), show¹⁶ sequentially evolving Domain Wall phases, from DW Vapour to DW Liquid to DW Crystal or oriented ‘twins’. The 3D physical picture is similar, but we show the earlier¹⁶ 64^2 2D system as illustrations.

Video A. The droplet in \vec{r} -space: This shows the coordinate-space evolution for $T_d > T > T_1$, for the Golf Hole type a) passage of Fig 1. Random initial martensite seeds rapidly form a single-variant DW Vapour droplet, enclosed in a martensite-austenite DW. This fluctuates like an amoeba, searching over incubation delays for a conversion passage to a DW Liquid, and then a quick symmetry-breaking to a DW crystal .

Video B. The droplet in \vec{k} -space: This shows the evolution as Video A but now in Fourier space, for $T_d > T > T_1$. The dynamic structure factor for variant spins $|S(\vec{k}, t)|^2$ is shown in (k_x, k_y) space, with elliptic contours of a DW Vapour going to the bi-diagonal X of a DW Liquid, and to a single-diagonal $k_y = -k_x$ line of a DW Crystal.

Videos C,D are in different quench regimes than A,B but are also given for completeness. *Video C. The \vec{r} -space dynamic catalysts:* This shows the evolution for deep quenches to $T \ll T_1$, of the facilitation type b) passage. The DW Vapour now converts rapidly to a sluggish DW Liquid of frozen walls. Transient hotspots of austenite in martensite act as dynamic catalysts, that unlock and

delete even far-off minority-diagonal DW segments, leaving a dominant-diagonal ,martensite-martensite DW crystal, or twins¹⁶.

Video D. The \vec{r} -space tweed precursor: This shows dynamical tweed in the above-transition region $T > T_d > T_1$, of an oscillating array of martensitic islands in austenite sea.

This might arise from a vibrating \vec{k} space profile of the droplet, attempting to enter a topologically blocked GH .

²¹ S. R. Shenoy and T. Lookman, Phys. Rev. B **78**, 144103 (2008), see Fig 7.

²² N. Shankaraiah, K.P.N. Murthy and S.R. Shenoy, unpublished.

²³ Another $N_{OP} = 2, N_V = 3$ kernel in 2D reproduces the self-similar star textures of lead orthovanadate. R. Vasseur, T. Lookman and S.R. Shenoy, Phys Rev B **82**, 094118, 92010 (2010); C. Manolikas and A. Amelinckx, Phys. Stat. Sol., **60**, 607 (1980); **61**, 179 (1980).

²⁴ U. Chandni, S Kar-Narayan, A. Ghosh, H.S. Vijaya and S. Mohan, Acta Mater., **57**,6113 (2009); A. Planes, Ll. Manosa and E. Vives, J. Alloys and Comp., **577**, S699 (2013);

X. Balandraud, N. Barrara, P. Biscarin, M. Grediac, G. Zanzotto, Phys. Rev. B, **91**,174111 (2015);

B. Blaysat, X. Balandraud, M. Grediac, E. Vives, N. Barrera and G. Zanzotto, Nature Commun. Mater., **1**,3 (2020);

Z. Eranson, B. Ruta, S. Hechler, M. Stolpe, E. Pineda, I. Gallimo, and R. Busch, Phys. Rev. Lett., **115**, 175701 (2015). See also Physics **8**, S5121 (2015).